



Stability of extended beam-to-girder shear tab connections under gravity induced shear force

Mohammad Motallebi¹, Dimitrios G. Lignos², Colin A. Rogers³

Abstract

Extended shear tab connections are widely used to connect beams to the webs of girders. In the full-depth configuration of extended beam-to-girder shear tabs, the shear plate is typically fillet welded to the web, as well as to the top and bottom flanges of the girder. Due to the extended nature of the shear tab, i.e. the connection to the beam is actually made well outside of the cross-section of the girder, the inelastic stability of this plate must be accounted for in design. A coordinated experimental and numerical investigation of the behaviour and stability requirements of full-depth extended shear tabs is described in the paper. The findings from a detailed finite element (FE) simulation of 3 single-sided beam-to-girder shear tab connections, tested at McGill University, are discussed. Based on the FE analyses, the load transfer mechanism and the buckling capacity of the stiffened portion of the full-depth shear tab were determined. The parameters, which influenced the buckling of the stiffener, were studied; including the depth and thickness of the shear plate, the depth of the girder, the width of the girder flanges, and the flexibility of the girder web. Further FE analyses were completed to determine the buckling capacity of the shear tab with reduced depth of the stiffener. In addition, the load-transfer mechanism and buckling capacity of these shear plates were modeled when they are used in double-sided configurations, i.e. when a beam is placed on both sides of the girder.

1. Introduction

Extended shear tab connections have been widely used to connect beams to girders due to their ease of erection and fabrication. As shown in Fig.1, the increased length of the extended shear tab allows the beam to be connected to the girder web without coping the beam flanges, which can be an expensive and time-consuming procedure. The shear plate usually is welded to both top and bottom flange in addition to the web of the girder. It was observed that this configuration decreases the out-of-plane bending demand on the girder web as compared to the other configurations with partial depth shear tabs, in which the shear plate is solely welded to the girder web or the top flange of the girder (Hertz et al. 2015). On one hand, plate buckling was

¹ Graduate Research Assistant, McGill University, <mohammad.motallebinasrabadi@mail.mcgill.ca>

² Associate Professor, Swiss Federal Institute of Technology, Lausanne (EPFL), <dimitrios.lignos@epfl.ch >

³ Associate Professor, McGill University, <colin.rogers@mcgill.ca >

determined as the governing failure mode of extended beam-to-girder shear tab connections with full depth shear plates (Sherman and Ghorbanpoor 2002, Goodrich 2005). On the other hand, there is a lack of guidance regarding the buckling strength of the full depth extended beam-to-girder shear tabs. The AISC design method (2011), originally developed for extended beam-to-column shear tabs, implements equations corresponding to the buckling strength of a doubly coped beam (Cheng et al. 1984) to determine the flexural buckling strength of the shear plate.

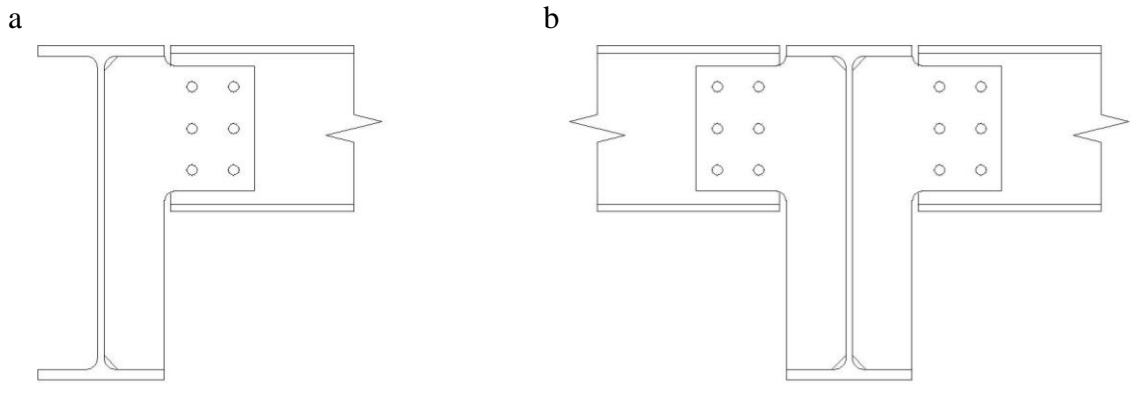


Figure 1-Full depth extended beam-to-girder shear tab connection: a) Single-sided shear tab connection, b) double-sided shear tab connection

In response to the lack of knowledge of the behaviour of extended beam-to-girder shear tabs, an extensive research program was conducted at McGill University (Hertz 2014, Goldstein 2015). During this research program, full-scale laboratory tests and complimentary finite element (FE) analyses were implemented to evaluate and improve the current design procedure for extended beam-to-girder shear tabs. This paper presents the results of finite element analyses conducted on models of full depth extended beam-to-girder shear tab connections. Their load transfer mechanism was determined in addition to their buckling strength. The parameters which influenced the buckling of the stiffener were studied, including; the depth and thickness of the shear plate, the depth of the girder and the width of the girder flanges. The effect of the flexibility of the girder web was studied by considering a double-sided configuration (Fig. 1b) in which a beam is framed to both sides of the girder.

2. Full-Scale Laboratory Testing

In order to better comprehend the behaviour of extended beam-to-girder shear tab connections, several full-scale laboratory tests were conducted at McGill University (Hertz 2014, Goldstein 2015). To ensure that these connection configurations are representative of current design practice in North America, they were designed in coordination with practicing structural engineers. As shown in Fig. 2, three specimens were selected to develop finite element models. A comparison between specimens BG1 and BG2 illustrated the effect of compactness of the stiffener. The slenderness ratio of the shear plate of specimens BG1 & BG3 ($b/t=11.4$ & 19.1 , respectively ('b' is the width of the stiffener as shown in Fig. 2)) does not satisfy the CSA-S16 (2014) requirement for compactness of a plate girder's stiffeners ($200/\sqrt{F_y} = 10.7$) while the stiffener of specimen BG2 satisfies this requirement ($b/t=8.5$). In addition, a comparison between specimens BG1 and BG3 demonstrated the effect of the ratio between the depth of the shear plate and the girder web height. The girder and beam were ASTM A992 Grade 50 ($F_y=345$ MPa) steel. ASTM A572 Grade 50 shear plates were snug-tightened to the beam using ASTM A325

bolts. To weld the shear tab to the supporting girder, an E71T ($F_u=490$ MPa) electrode was used through the flux-cored arc welding process with additional shielding gas (CO₂). Details of the test setup are summarized in Hertz (2014) and Hertz et al. (2015).

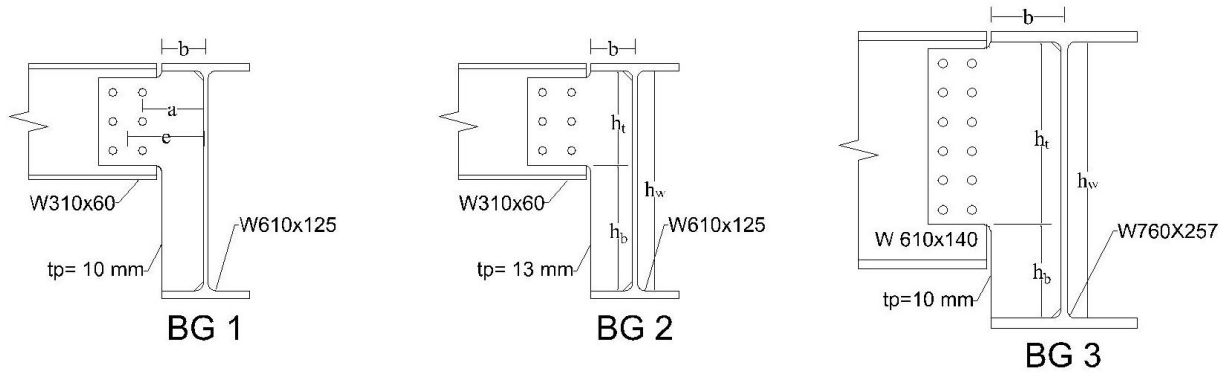


Figure 2-Test specimen details

3. Finite Element Simulation

Finite element simulation was adopted to obtain a deeper understanding of the behaviour of extended beam-to-girder shear tab connections. To develop reliable FE models in Abaqus of the tested specimens, all features of the models including geometry, boundary conditions, material properties, element size and element type, contacts and interactions, and the loading protocol were chosen to be representative of the real situation of the laboratory tests. A complete description of the finite element models was provided by Motallebi et al. (2016).

The numerical modelling predictions are presented along with the experimental measurements in Fig. 3. Among others, the developed shear force of the connection and the out-of-plane deformation of the girder web were chosen as the critical criteria for verification. The comparison between the numerical predictions and the test measurements for the connection shear force shows that the calculation of the numerical model deviated from the test measurements in the initial increments of loading. This discrepancy arises from the different contact situation between the bolt shanks and the bolt holes in the model and in the laboratory. The shear tab connections were snug-tightened in which bearing between the bolt shanks and bolt holes transfers the shear force between the beam and the shear plate. Therefore, the initial response of a snug-tightened connection depends greatly on the contact between bolts shank and bolt holes. Since the contact situation in the tests could not be accurately measured, in the FE model the bolts were placed at the centre of bolt holes, resulting in a 1mm gap around the entire perimeter. Furthermore, the finite element model of the BG3 specimen slightly overestimated the level of shear force corresponding to the point of stiffness degradation. This discrepancy can be attributed to the specimen's sensitivity to the local imperfections of the shear plate due to its high slenderness ratio. As exact imperfections of the connection components were not available, the local imperfections for the shear plate and the girder web as well as the flanges of the girder were proportioned to the limits of manufacturing tolerances for the web and flange of W section (CISC 2010), respectively. Regarding the out-of-plane deformation of the girder web, the numerical models predict reasonably well.

3.1 Results of Finite Element Models

As shown in Fig. 3, the connection shear force and the out-of-plane deformation of the girder web are presented versus beam rotation. The test measurement and the predictions of the numerical models of single-sided shear tab connections (EXP-S.S and F.E-S.S, respectively) are presented along with the predictions of the finite element models with double-sided shear tabs (F.E-D.S), where a beam is framed to both sides of the girder. It should be noted that the comparison between results of single and double-sided shear tabs demonstrates the contribution of the out-of-plane stiffness and strength of the girder web to the behaviour of single-sided shear tabs. To decrease computational costs, symmetric boundary conditions were implemented along the girder axis, and a beam and half of girder section were included in FE models of double-sided shear tabs.

For the single-sided shear tab connection of the BG1 specimen, yielding began at the neck of the shear plate at a shear force equal to 98 kN corresponding to 1.30% of beam rotation. The slope of the representative curves for out-of-plane deformation of the girder web and shear plate increased significantly at 180 kN shear force (1.85% rotation). The stiffness of the connection decreased at 228 kN shear force, which corresponds to about 2.3% beam rotation when yielding propagated through the full width of the stiffened section of the shear plate, which is confined between the flanges and the web of the girder. Then, the web of the girder began to yield at 239 kN shear force (i.e., 2.91% beam rotation). The slope of the out-of-plane deformation of the shear plate (LVDT4) increased again at 259 kN shear force (5.77% beam rotation). For the double-sided shear tab connection of the BG1 specimen, the onset of yielding occurred at the neck of the shear plate at 166 kN (1.51%), but its out-of-plane deformation remained negligible. Unlike the single-sided connections, the yielding propagated along the bolt line instead of the stiffened part of the shear plate. The stiffness of the connection decreased significantly at 2.25% rotation (301 kN) when the total height of the shear plate along the bolt line yielded. Yielding then propagated to the stiffened section of the shear tab in the vicinity of girder top flange due to bending moment. Although the slope of the curve representative of LVDT4 deformation increased significantly at 6.06% rotation (421 kN), its out-of-plane deformation remained small.

Regarding specimen BG2, yielding began at the neck of the shear plate at a shear force of 146 kN (beam rotation of about 1.90%). The stiffness of the connection started to decrease slightly at 231 kN (2.54% beam rotation) while yielding was propagating through the stiffened portion of the shear tab. The web of the girder began to yield at 320 kN (3.63% rotation) while the slope of the representative curves for out-of-plane girder web deformation increased significantly. The slope of the out-of-plane deformation of the shear plate (LVDT4) increased significantly at 381 kN shear force (4.90% beam rotation). The shear plate yielded along the interior bolt line at a shear force equal to 427 kN corresponding to 6.46% beam rotation. For the double-sided shear tab of the BG2 specimen, yielding of the beam web governed the response of the connection. As the behaviour of the shear tab connection is the main interest of this study, the results of the finite element model containing a beam with elastic material properties were presented in Figs. 4c&d. The onset of yielding was observed at the neck of the shear plate at 225 kN (2.11%). Similar to the double-sided shear tab of BG1 specimen, the yielding propagated along the bolt line instead of the stiffened part of the shear plate. The total height of shear plate along the bolt line, closest to the girder, yielded at 2.88% rotation (372 kN) while the stiffness of the connection started to decrease. The connection reached its plateau of strength at 630 kN shear

force which corresponds to 7.84% beam rotation. The bottom flange of the beam started to bind on the shear plate at a shear force equal to 635 kN (8.83%). The out-of-plane deformation of the shear plate remained small during the analysis.

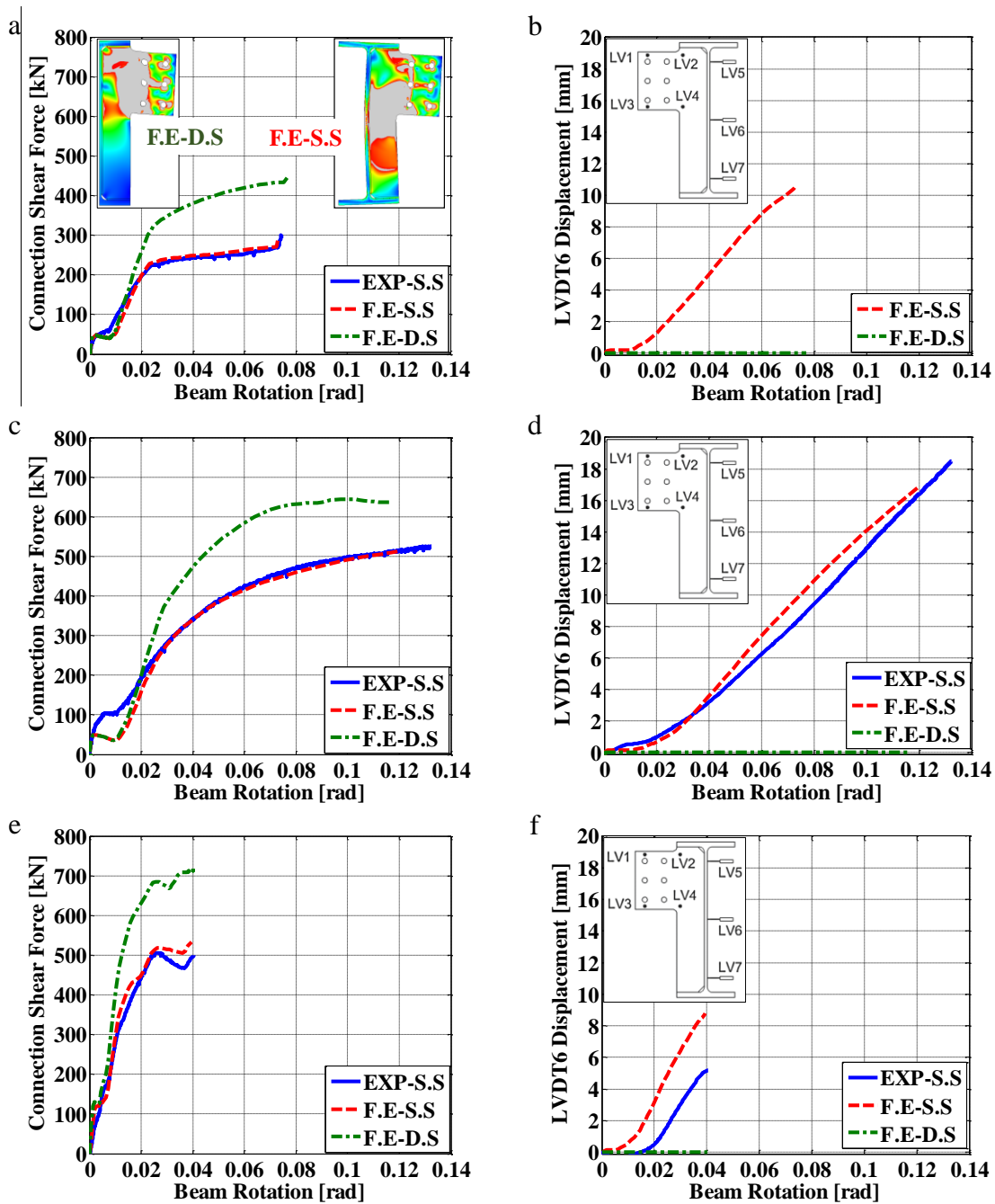


Figure 3-Response of FE models for: a) shear force versus beam rotation of specimen BG1, b) out-of-plane deformation of girder web versus beam rotation of specimen BG1, c) shear force versus beam rotation of specimen BG2, d) out-of-plane deformation of girder web versus beam rotation of specimen BG2, e) shear force versus beam rotation of specimen BG3, f) out-of-plane deformation of girder web versus beam rotation of specimen BG3.

For the BG3 Specimen, the finite element model began to yield at the neck of the shear plate at 163 kN shear force, which corresponds to a beam rotation of 0.72%. The yielding then

propagated through the full width of the stiffener at 369 kN shear force corresponding to 1.24% beam rotation. At this point a decrease in the stiffness of the connection initiated. The out-of-plane deformation of the girder web and the shear plate started to increase rapidly at 389 kN shear force (1.34% beam rotation). The stiffness of the connection decreased significantly at 430 kN shear force corresponding to a beam rotation equal to 1.65%. The onset of yielding of the girder web occurred at 446 kN shear force (1.96% beam rotation). The connection reached its peak value for shear force at 518 kN (2.74% rotation). The binding between the beam bottom flange and the shear plate occurred at 505 kN shear force (3.63% beam rotation). Yielding propagation and out-of-plane deformation of the shear plate are shown in Fig.4.

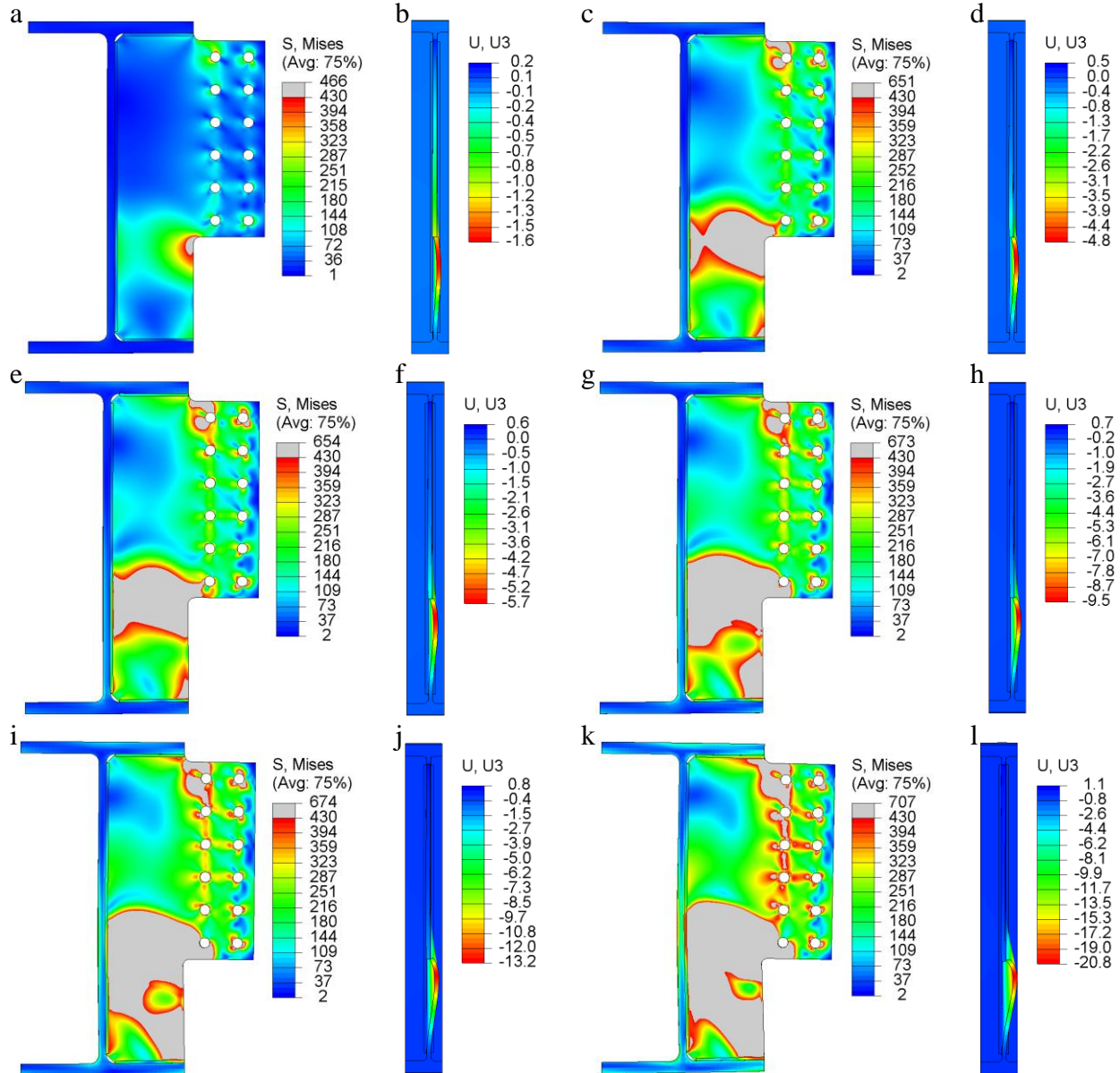


Figure 4-FE model predictions of specimen BG3 (single sided shear tab): a) stress at $\theta=0.74\%$, b) out-of-plane deformation at $\theta=0.74\%$, c) stress at $\theta=1.24\%$, d) out-of-plane deformation at $\theta=1.24\%$, e) stress at $\theta=1.34\%$, f) out-of-plane deformation at $\theta=1.34\%$; g) stress at $\theta=1.65\%$, h) out-of-plane deformation at $\theta=1.65\%$, i) stress at $\theta=1.96\%$, j) out-of-plane deformation at $\theta=1.96\%$, k) stress at $\theta=2.74\%$, l) out-of-plane deformation at $\theta=2.74\%$, (The gray colour represents yielded regions)

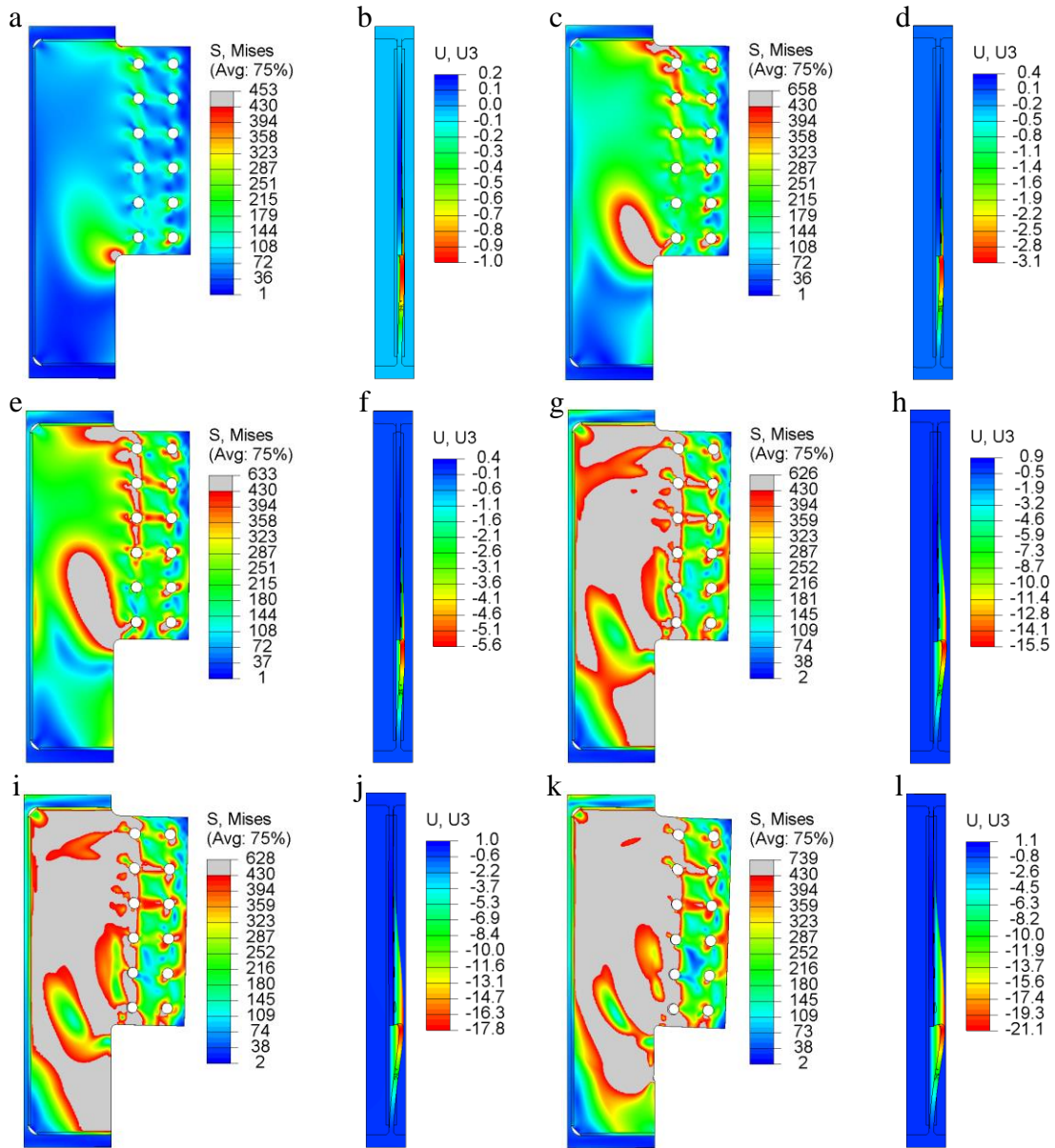


Figure 5- FE model predictions of specimen BG3 (double sided shear tab): a) stress at $\theta=0.72\%$, b) out-of-plane deformation at $\theta=0.72\%$, c) stress at $\theta=1.14\%$, d) out-of-plane deformation at $\theta=1.14\%$, e) stress at $\theta=1.47\%$, f) out-of-plane deformation at $\theta=1.47\%$; g) stress at $\theta=2.46\%$, h) out-of-plane deformation at $\theta=2.46\%$, i) stress at $\theta=2.70\%$, j) out-of-plane deformation at $\theta=2.70\%$; k) stress at $\theta=3.08\%$, l) out-of-plane deformation at $\theta=3.08\%$, (The gray colour represents yielded regions)

For the double-sided model of specimen BG3, yielding initiated at the neck of the shear plate at 234 kN shear force (0.72% beam rotation). The stiffness of the connection decreased slightly at a shear force equals to 470 kN (1.14% beam rotation). The slope of the curve representing the out-of-plane deformation of the shear plate increased significantly at 561 kN shear force (1.47% beam rotation) and resulted in significant decrease in the stiffness of the connection. The connection reached its plateau of the strength at 682 kN shear force (2.46% beam rotation), while

a large portion of the stiffened portion of the shear plate yielded in addition to its net section along the bolt line, closest to the girder. The shear force reached its peak value at 684 kN (2.70% beam rotation). The binding between beam bottom flange and the shear plate occurred at 668 kN shear force (3.08% beam rotation). The yielding propagation in the shear plate is presented in Fig. 5, along with the out-of-plane deformation of the shear plate.

3.2 Comparison and Discussion of Finite Element Results

Results of the laboratory tests and the complementary finite element simulations demonstrated that single-sided and double-sided shear tabs have different failure mechanisms. Double-sided configurations of specimens BG1 and BG2 experienced shear forces (430 kN and 630 kN, respectively), which were close to their net section fracture limits (482 kN and 643 kN for BG1 and BG2 specimens, respectively). However, specimen BG3 reached its plateau of the strength at 682 kN shear force, which is much lower than its net section fracture limit (915 kN). Unlike specimens BG1 and BG2, the double-sided connection of specimen BG3 experienced yielding and out-of-plane deformation at the stiffened portion of its shear plate, which resulted in failure at a shear force lower than its net section fracture limit. Yielding and large out-of-plane deformation were observed at the stiffened part of the single-sided shear tabs. Due to the complex behaviour of the shear tab connections, additional finite element simulations were carried out on models with elastic material properties. The findings from these models were used as a baseline for understanding the force transfer mechanism and the elastic buckling of shear tab connections. As shown in Fig. 6, the buckling strength of single-sided shear tabs was lower than the buckling strength of the corresponding double-sided shear tabs. Furthermore, the finite element models show that buckling occurs in the stiffened part of the shear plate.

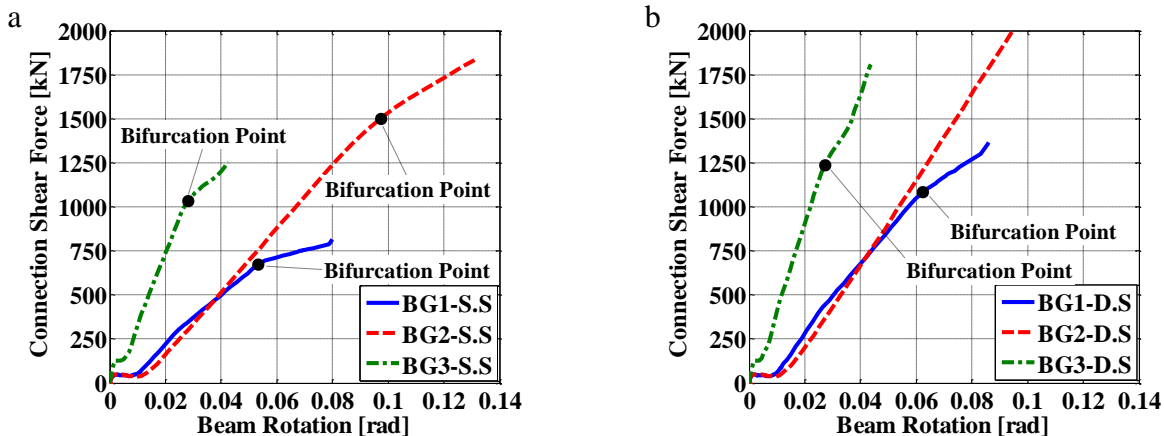


Figure 6-Predictions of FE models with elastic material properties for: a) single-sided shear tabs, b) double-sided shear tabs.

The free body cut option of the Abaqus software was implemented to determine directly the forces and moments (Fig. 7), which were developed in all components of a connection's FE model. The vertical component of the forces developed through different sections of the shear plate are presented in Fig. 8.

As shown in Fig. 8a, a large component of the connection shear force (i.e. Cut #9 (C9)) was transferred to the girder web (i.e. Cut#11 (C11)) as a shear force, while the girder flanges (Cut#10 (C10) and Cut#14 (C14)) carried 20% of the connection shear. It should be noted that

the shear force was not distributed uniformly over the depth of the girder web, which is in contrast with the assumptions made in the design procedure of extended beam-to-girder shear tab connection (AISC 2011). As shown in Figure 8c, the shear force along the top of the stiffener (CUT#11Top (C11T)) developed downward to counterbalance the moment mobilized due to the existing eccentricity of the shear force. To counterbalance the resultant of the downward forces, a compressive axial force was developed in the stiffener with a greater magnitude as compared to the applied shear force. This compressive axial force was balanced by an upward shear force, which is mobilized along the bottom portion of the stiffener (Cut11Bottom (C11B)). As shown in Figure 8e, the slope of the curve representing the axial force of the stiffener decreased significantly at 1125 kN compression corresponding to a connection shear force equal to 672 kN which was considered as a bifurcation point of elastic buckling.

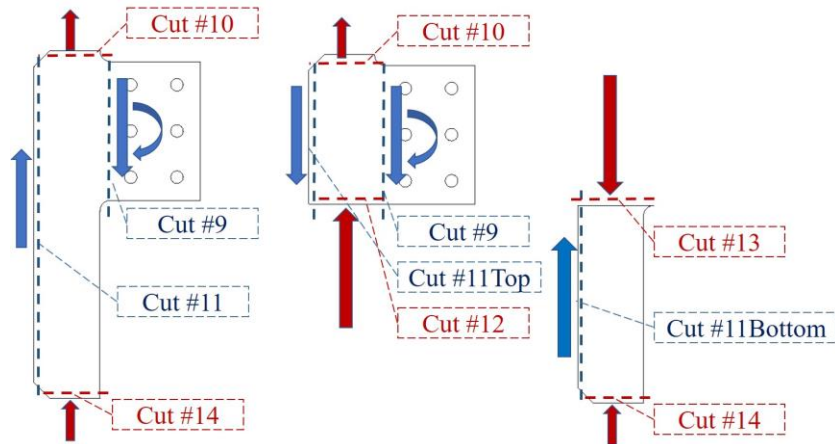


Figure 7- Free body cuts through shear plate

A comparison between Figs. 8a & 8b demonstrated that the girder top flange of double-sided connections resisted a larger portion of shear force as compared to a single-sided shear tab. The top flange of the girder carried 20% of the connection shear force while the bottom flange negligibly contributed to transfer the connection shear force. As shown in Fig. 8d, unlike the single sided shear tab, the shear force at the top portion of the stiffener of the double-sided shear tab was an upwards force that counterbalanced a significant portion of the connection shear force. Its stiffener therefore was subjected to a smaller level of compression force, although the double-sided connection was subjected to a larger shear force in comparison to the single-sided shear tab. The stiffener buckled at 508 kN compression force, corresponding to 1084 kN shear force, which is half the buckling force observed in the single-sided shear tab. This observation is attributed to the fact that the critical section of the stiffener, along the bottom edge of the extended portion of the shear plate, was subjected to a larger horizontal shear stress. As shown in Fig. 9, the stiffener was subjected to the bending moment due to existing eccentricity of the shear tab connection. Regarding the top part of the stiffener of the single-sided shear tab (Fig. 9a), this moment was counterbalanced to a great extent by the downward shear force along and a couple of horizontal shear forces. Due to low out-of-plane stiffness of the girder web, its contribution to resisting the bending moment was negligible.

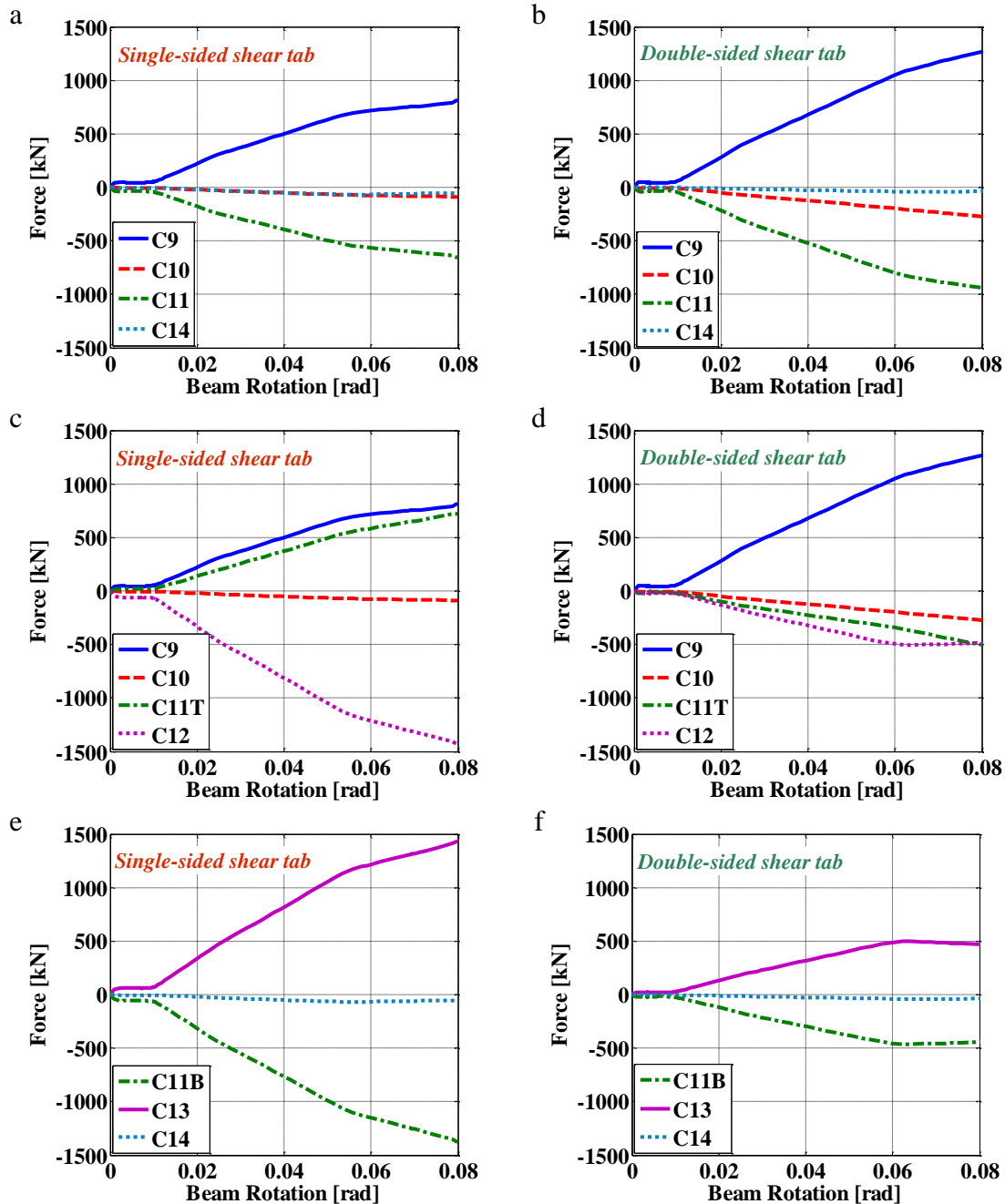


Figure 8- Prediction of elastic FE models of specimen BG1 for vertical force at: a) the stiffener single-sided connection, b) the stiffener of double-sided connection, c) the top part of the stiffener of single-sided connection, d) the top part of the stiffener of double-sided connection, e) the bottom portion of the stiffener of single-sided connection, f) the bottom portion of the stiffener of double-sided connection.

In comparison to single-sided shear tab connections, the inflection point of the double-sided shear tab connections (Fig. 9b) formed further from the girder, due to its higher stiffness. Furthermore, the connection shear force (Cut#9) and the upward shear force along the top part of the stiffener (Cut#11Top) formed a couple of shear forces and applied an extra moment on the stiffener. This large bending moment was resisted by the moment of the girder web and a moment couple resulting from the horizontal shear forces. Therefore, the stiffener of the double-

sided shear tab was subjected to a much higher horizontal shear force as compared to the single-sided shear tab.

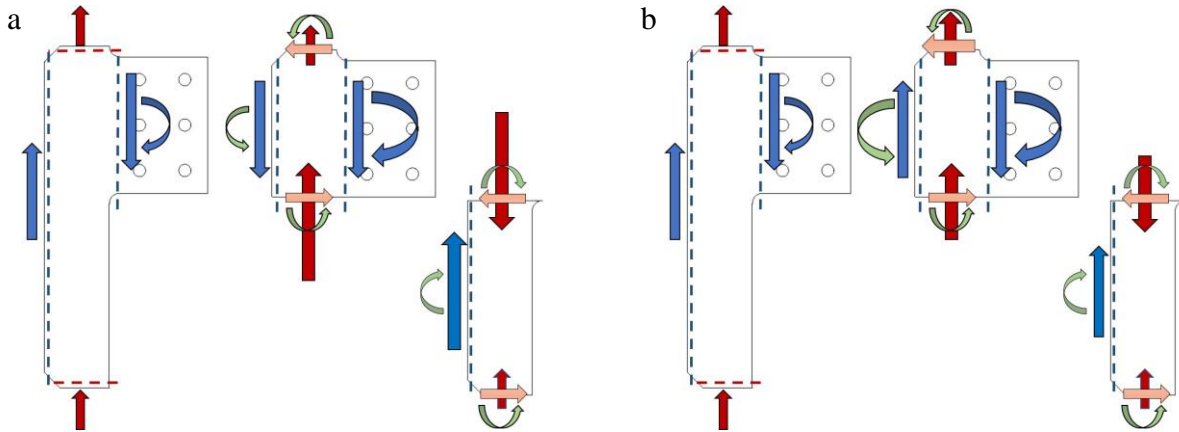


Figure 9-Free body diagram of specimen BG1 for: a) single-sided shear tab, b) double-sided shear tab.

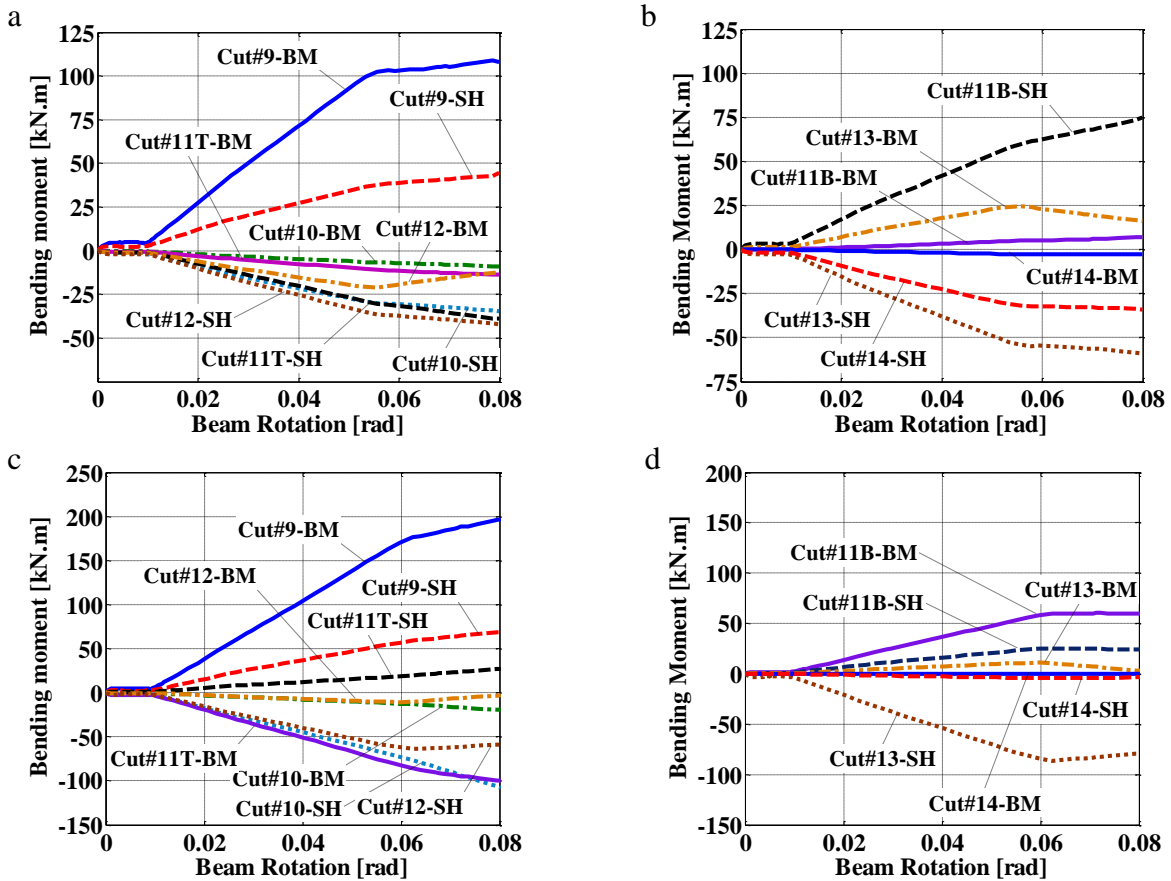


Figure 10-FE model prediction of specimen BG1 for bending moment at: a) the top part of the stiffener of the single-sided connection, b) the bottom part of the stiffener of the single-sided connection, c) the top part of the stiffener of the double-sided connection, d) the bottom part of the stiffener of the double-sided connection. (The suffix '-BM' refers to the bending moment at section while the suffix '-SH' refers to the bending moment, calculated by projecting the shear force of each section at the centre of the corresponding portion of the stiffener)

The bending moment developed in the top and bottom portions of the stiffener of specimen BG1 (Fig. 10) demonstrated that greater horizontal shear force was mobilized at the critical section of the double-sided shear tabs (Figs. 10c & 10d) in comparison to the single-sided shear tabs (Figs. 10a & 10b). In comparison to the single-sided shear tab, the larger horizontal shear force resulted in a 50% decrease of the axial force corresponding to the elastic buckling of the stiffener of the double-sided shear tab. In other words, the interaction of axial and shear forces at the critical section of the stiffened portion of the shear tab resulted in elastic buckling of the shear tab. However, this interaction of axial and shear forces is not considered in current AISC's design equations for the buckling of shear tabs.

A comparison between results of the elastic model of specimens BG1 and BG3 (Fig. 8 and Fig. 11) demonstrated the effect of the depth of the shear plate and the height of the girder web. The ratio between the height of the top part of the stiffener and the height of the girder web (h_t/h_w), as shown in Fig. 2, represents the relative distance between the bottom edge of the extended portion of the shear plate and the bottom flange of the girder. As this ratio approaches unity, the bottom edge of the extended portion of the shear plate becomes closer to the bottom flange of the girder. Therefore, the stiffener can mobilize higher shear stress along the bottom edge of the extended portion of the shear plate to counterbalance a larger part of the bending moment, applied to the stiffener due to existing eccentricity of the shear tab connection. As shown in Fig. 11, the elastic model of specimen BG3 needed a smaller fraction of the connection shear force to be mobilized upward along the top part of the stiffener (Cut#11Top). This smaller upward shear force in the top portion of the stiffener led to a smaller axial compressive force through the critical section of the stiffener, along the neck of the shear plate.

Furthermore, yielding of the shear plate affects the loading transfer mechanism of the shear plate. As shown in Fig. 11, the stiffener of specimen BG3 lost its compression resisting capacity as soon as it experience yielding. The post yielding behaviour of the stiffener depends greatly on its slenderness. As mentioned before, the slenderness ratio of the shear plate of specimen BG1 does not satisfy the CSA-S16 (2014) requirement for compactness of a plate girder's stiffeners while the stiffener of specimen BG2 satisfied this requirement. Due to the greater compactness of the stiffener in specimen BG2, the connection was able to continue resisting shear after yielding of the stiffener. In contrast, the BG1 connection reached its plateau of strength soon after yielding of the stiffener. In addition, the BG3 specimen, containing a stiffener with the largest slenderness ratio, significantly lost its ability to transfer shear force soon after the yielding of its stiffener.

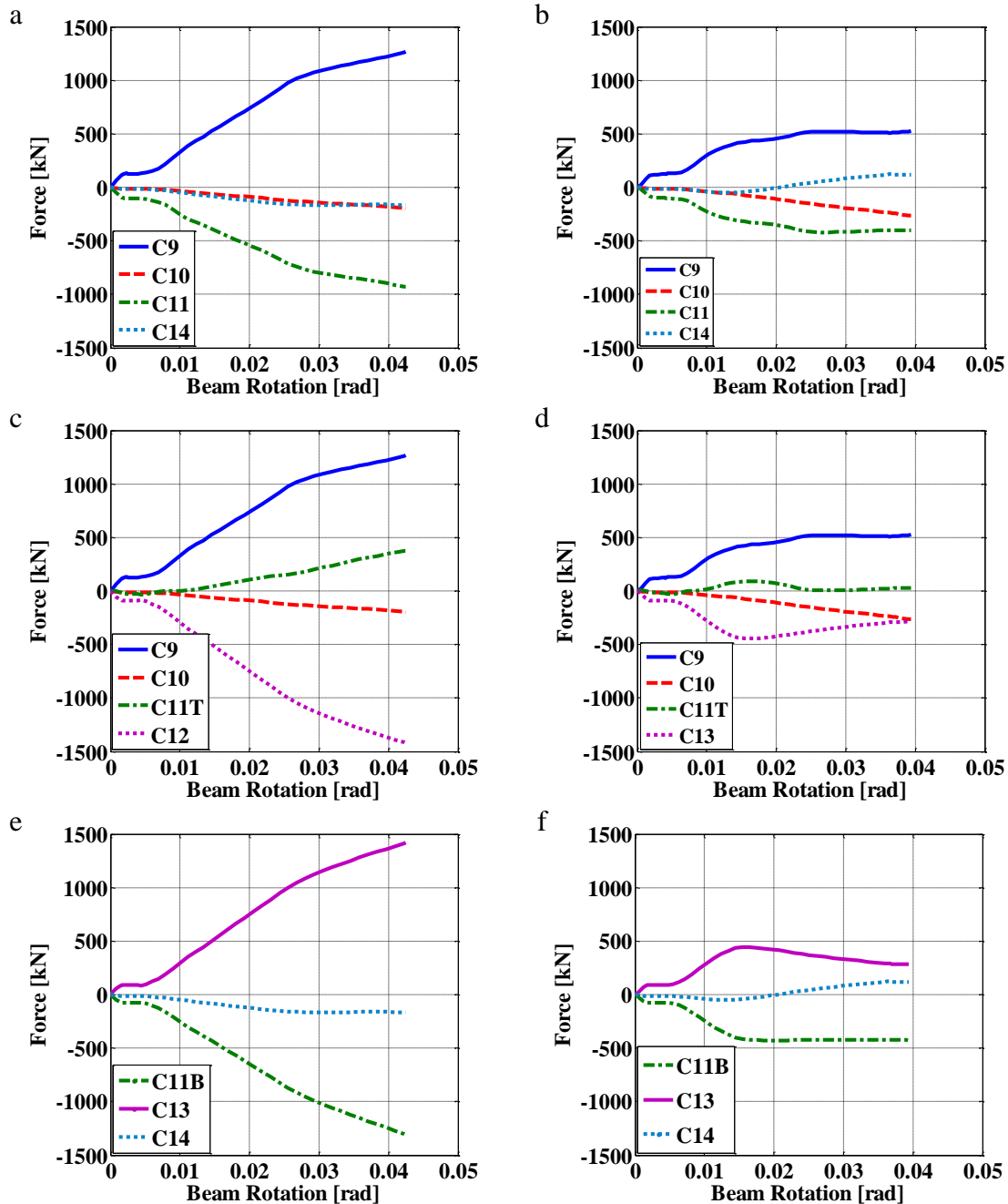


Figure 11-Prediction of finite element models of single-sided connection of specimen BG3 for vertical force at: a) the stiffener of elastic model, b) the stiffener of model with yieldable components, c) the top part of the stiffener of the of elastic model, d) the top part of the stiffener of the model with yieldable components, e) the bottom part of the stiffener of the elastic model, f) the bottom part of the stiffener of the model with yieldable components

4. New Detailing of Shear Tab

The results of the finite element models of the extended beam to girder shear tabs with full depth shear plates demonstrated negligible contribution of the bottom flange of the girder to resist the connection shear force. Although the horizontal shear force at Cut#14, as shown in Figs. 10 b & d, played an important role to satisfy the equilibrium of the bending moment at the bottom part of the stiffener, a negligible amount of the connection shear force was transferred to the bottom

of the girder as an axial force through this section, as shown in Figs. 8e & 8f. This behaviour raised doubt as to the benefit of extending the shear plate to the bottom flange of the girder. Furthermore, the fabrication of this type of full height shear tab is a time consuming procedure, which often requires repeated grinding of the stiffener such that it fits snugly between the inner surfaces of the girder flanges. To solve this problem and to obtain a more economical connection, the authors of this paper suggest a new detail for extended shear tab connections. As shown in Fig. 12, the shear plate is extended up to the bottom K-area region of the girder, which facilitates the fabrication procedure without substantially altering the force transfer in the connection. The K-area of the girder has adequate stiffness to develop the horizontal shear force near the bottom edge of the stiffened portion of the shear plate.

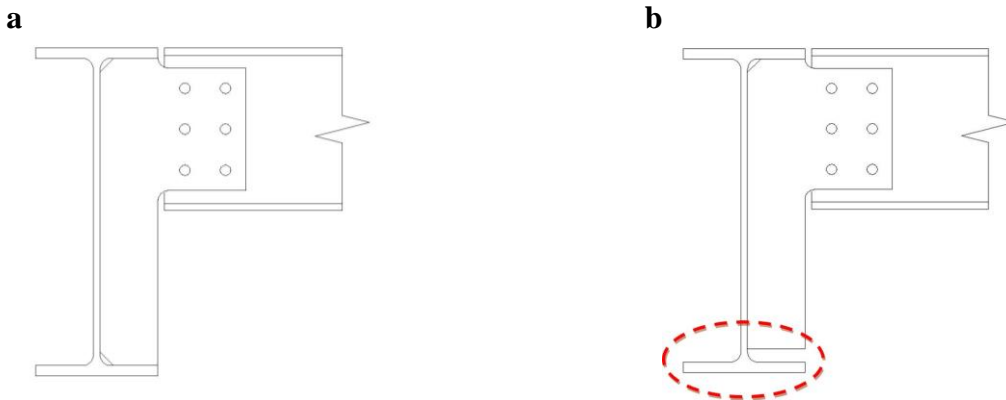


Figure 12-Full depth extended beam-to-girder shear tab: a) current detailing, b) proposed detailing

4.1 Finite Element Simulation Results

The force carrying efficiency of the proposed detailing was evaluated through finite element simulations. The finite element simulation results for the connection with the new detailing (suffix -N.D) is presented along with the regular connections (Fig. 12a) in Fig.13.

For the single-sided connection of specimen BG1 with new detailing (-S.S-N.D), the onset of yielding occurred at the neck of the shear plate at 103 kN shear force (1.43 beam rotation). Yielding, then, propagated through the full width of the shear plate at a shear force equal to 212 kN (2.25% beam rotation), while the stiffness of the connection decreased significantly. Yielding of the girder web started at its mid-depth at 234 kN shear force (3.00% beam rotation) when the connection reached its plateau of strength. The slope of the curve representing the out-of-plane deformation of the shear plate increased significantly at 235 kN shear force (4.00 % beam rotation). The girder web began to yield close to the bottom flange of the girder at 240 kN shear force (5.64% beam rotation). The binding between the bottom flange of the beam and the shear plate occurred at 249 kN shear force, which corresponds to 7.20% beam rotation. On the other hand, the double-sided connection with new detailing (-D.S-N.D) began to yield at the neck of the shear plate at 152 kN shear force (1.51 % beam rotation). The yielding propagated along the net section of the shear plate closest to the girder at 307 kN shear force (2.41% beam rotation) when the stiffness of the connection decreased significantly. Yielding propagated along the whole width of the shear plate at 372 kN shear force (4.28% beam rotation) while the slope of the curve representing the out-of-plane deformation of the shear plate increased significantly. The connection reached to its plateau of the strength at 384 kN shear force (5.16% beam rotation) while a large part of the shear plate yielded.

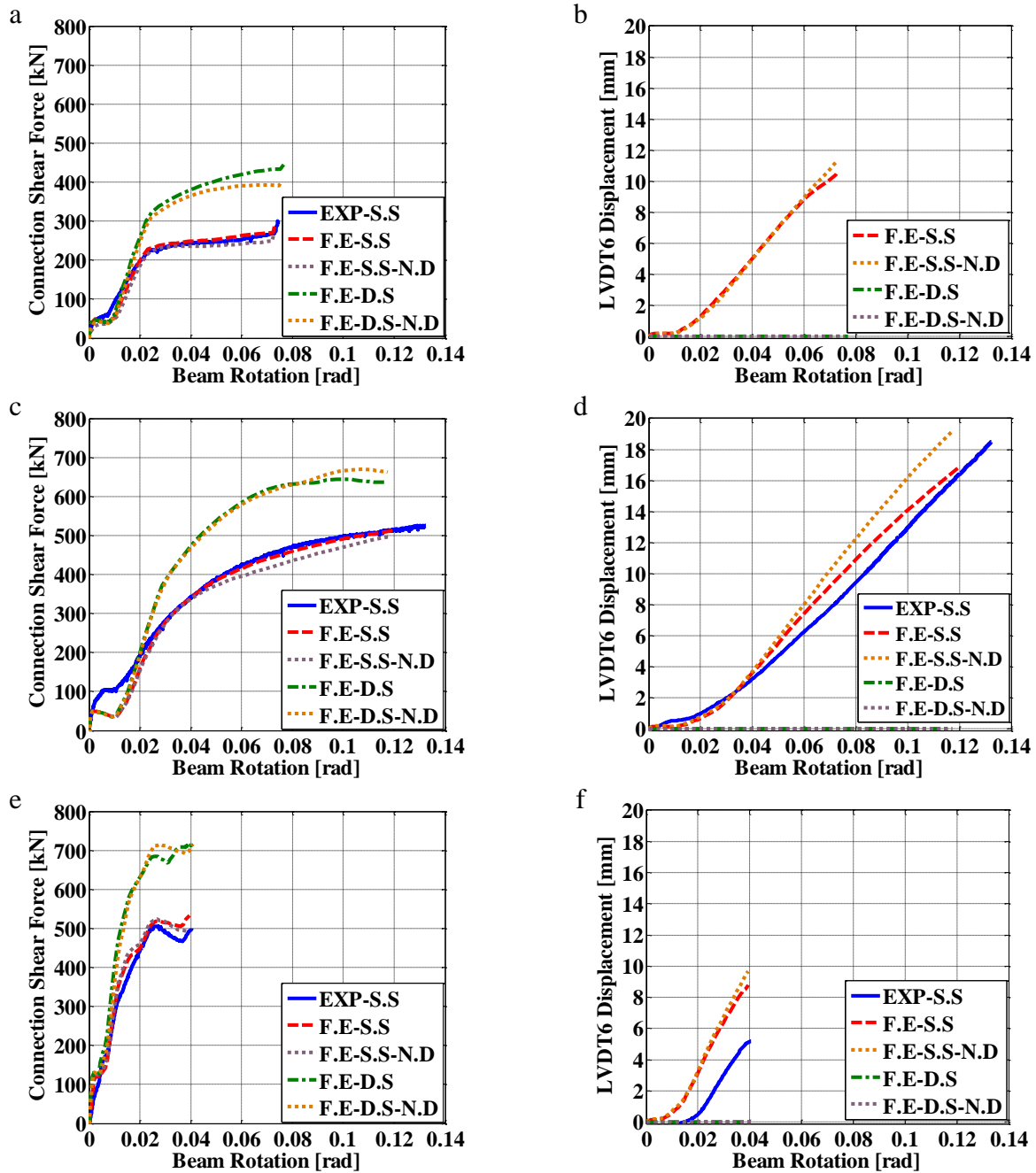


Figure 13-Response of FE models with full height and reduced height stiffener: a) shear force versus beam rotation of specimen BG1, b) out-of-plane deformation of girder web versus beam rotation of specimen BG1, c) shear force versus beam rotation of specimen BG2, d) out-of-plane deformation of girder web versus beam rotation of specimen BG2, e) shear force versus beam rotation of specimen BG3, f) out-of-plane deformation of girder web versus beam rotation of specimen BG3.

The single sided connection of specimen BG2, in which the new detailing was incorporated, began to yield at the neck of the shear plate at 129 kN shear force (rotation of 1.86% beam rotation) and the stiffness of the connection started to decrease slightly at 229 kN (2.56% beam rotation) when yielding propagated through the width of the stiffener. The web of the girder began to yield near the bottom K area at 249 kN (2.74% beam rotation) while its mid-depth

yielded at 323 kN (3.70% beam rotation) and the slope of the representative curves for out-of-plane deformation of the girder web increased significantly. The yielding moved through the full width of the shear plate at 307 kN shear force (3.43% rotation). The slope of the out-of-plane deformation of the shear plate (LVDT4) increased significantly at 379 kN shear force (5.25% rotation). The shear plate yielded along the interior bolt line at a shear force equal to 419 kN corresponding to 7.17% beam rotation. Regarding the double-sided connection of the BG2 specimen, all components of the connection in this model were defined to experience yielding, except for the beam, which was assigned elastic material properties. The onset of yielding was observed at the neck of the shear plate at 213 kN (2.08%), but its out-of-plane deformation was negligible. The total height of shear plate along the interior bolt line yielded at 3.14% beam rotation (397 kN) and the stiffness of the connection started to decrease at this point. The connection reached to its plateau of strength at 627 kN shear force which corresponds to 7.79% beam rotation. The bottom flange of the beam started to bind the shear plate at a shear force equal to 640 kN (8.67%).

For the single-side connection of specimen BG3, the shear plate began to yield at its neck and bottom edge at 176 kN shear force which corresponds to a beam rotation of 0.74%. Then the stiffness of the connection began to decrease at 359 kN shear force corresponding to 1.14% beam rotation, while yielding was propagating through the stiffener. In addition to the bottom K-area of the girder, yielding propagated through the full width of the shear plate at 406 kN shear force (1.37%). The out-of-plane deformation of the shear plate started to increase rapidly at 429 kN shear force (1.48% beam rotation) when the connection stiffness degraded by more than 50% compared to the elastic stiffness. The slope of the representative curve for the out-of-plane deformation of the girder web increased at 446 kN (1.68% beam rotation) significantly. The mid-depth of the girder started to yield at 460 kN shear force (1.99% beam rotation). Then the connection reached the peak value of its shear resistance at 524 kN (2.67% beam rotation), followed soon thereafter by a gentle decrease in resistance. Propagation of yielding through the girder web is shown in Fig. 14.

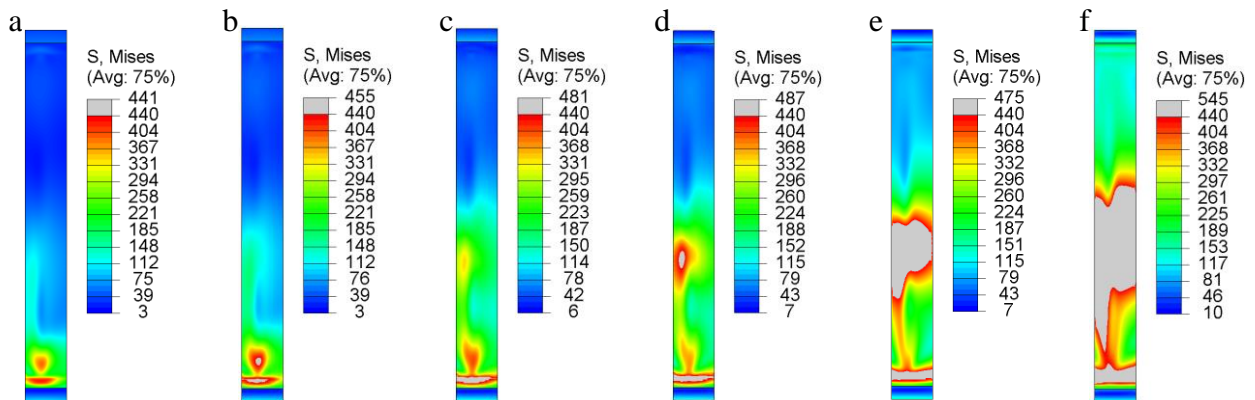


Figure 14- Predictions of FE model of specimen BG3 for stress of the girder web at: a) $\theta=1.16\%$, b) $\theta=1.37\%$, c) $\theta=1.78\%$, d) $\theta=1.99\%$, e) $\theta=2.67\%$, f) $\theta=3.93\%$ (end of analysis), (The gray colour represents yielded regions)

For the double-side configuration of specimen BG3, the shear plate started to yield at its neck at 228 kN shear force (0.77% beam rotation). The stiffness of the connection decreased slightly at a shear force equal to 465 kN (1.22% beam rotation). The stiffness, then, decreased significantly at 562 kN shear force (1.56% beam rotation). The slope of the curve representing the out-of-plane

deformation of the shear plate increased significantly at 602 kN shear force (1.77% beam rotation). The net section of the shear plate, closest to the girder, also yielded at this point. The connection reached its plateau of the strength at 711 kN shear force (2.56% beam rotation), while a large section of the stiffened portion of the shear plate yielded. The shear force reached its peak value at 716 kN (2.80% beam rotation), and binding between beam bottom flange and the shear plate occurred at 692 kN shear force (3.75% beam rotation).

4.2 Comparison and Discussion

A comparison of the responses of the connections with the new detailing with the specimens with the current detailing demonstrates the reasonable behaviour of the reduced height stiffener. As shown in Fig.13a, implementation of the reduced height stiffener in the single-sided configuration of the BG1 specimen resulted in a minor decrease of the connection strength (7%), while the out-of-plane deformation of the girder web (Fig. 13b) increased by 10%. In comparison with the single-sided configuration, the double-sided configuration of specimen BG1 experienced larger degradation in the shear capacity (9% of connection shear force) due to the reduced height stiffener. This observation can be attributed to the fact that the lack of contact between the bottom flange of the girder and the reduced height stiffener resulted in the mobilization of a larger horizontal shear force at the critical section of the stiffener in order to satisfy the bending equilibrium at the bottom portion of the stiffener. This higher demand of horizontal shear force in the reduced height stiffener caused its yielding at a lower level of connection shear force as compared to the connection with the full height stiffener.

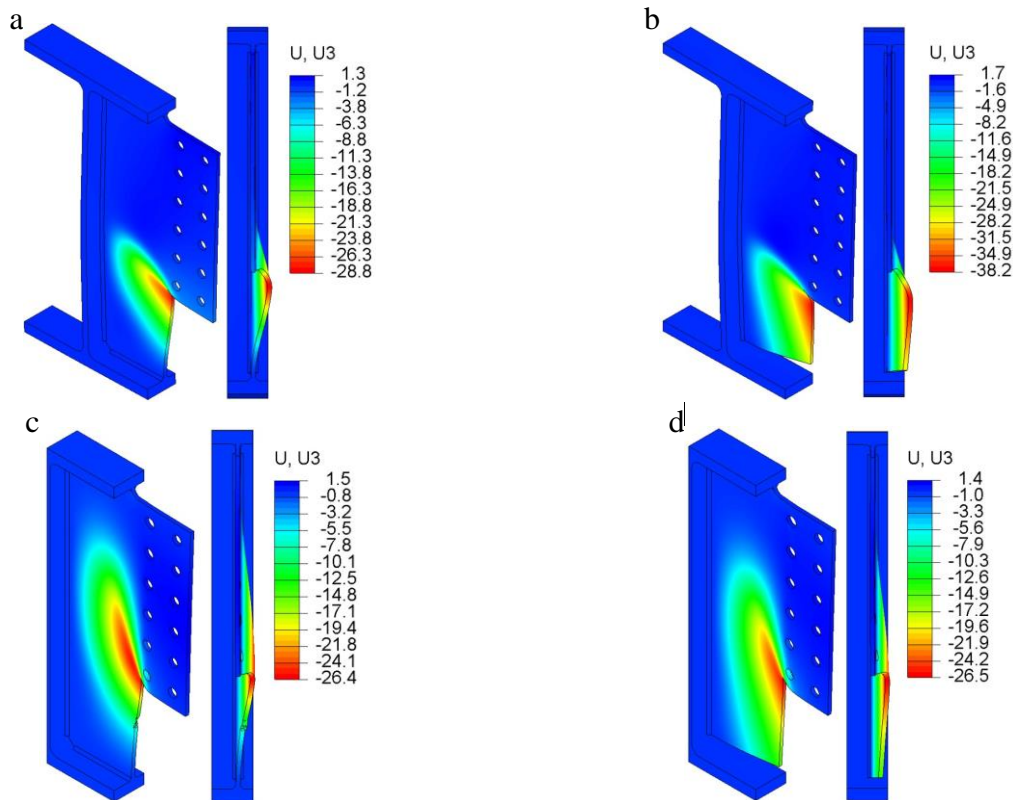


Figure 15- F.E. model predictions of specimen BG3 for out-of-plane deformation of the shear plate at: a) single-sided connection with full height stiffener, b) single-sided connection with reduced height stiffener, c) double-sided connection with full height stiffener, d) double-sided connection with reduced height stiffener.

Furthermore, yielding of the web of the girder, close to its bottom flange, resulted in larger out-of-plane deformation of the girder web in single-sided connections with the new detailing. Since the bottom edge of the stiffened part of the shear plate is free in the new detailing, its out-of-plane deformation is larger in comparison to connections with the current detailing, as shown in Fig. 15. Therefore, implementation of the requirement for a compact shear plate is more critical for a connection with the new detailing. The ability of compact shear tabs to continue resisting shear after yielding of the stiffener provide enough deformation to mobilize the top flange of the girder and load redistribution among connection components. Due to this fact, as shown in Fig. 13c, the implementation of a compact reduced height stiffener in specimen BG2 did not affect noticeably its shear capacity compared to the connection with a full height stiffener.

4. Conclusions

This paper contains a presentation of the results of finite element simulations of extended beam-to-girder shear tab connections with full depth shear plates. Comparison between the predictions using finite element simulation and the measured response of test specimens demonstrates the reasonable accuracy of a numerical model to detect failure modes of shear tab connections, among others, yielding of shear plate and girder, out-of-plane deformation of the girder web and the shear plate. The major findings of this study are summarized as follows:

- Regarding the single-sided configuration of full depth extended beam-to-girder shear tab, the critical section of the stiffened portion of the shear plate (section along the bottom edge of the extended part of the shear plate) was subjected to high axial and shear force resulting in local yielding of shear plate and degradation of the connection stiffness.
- The buckling of full depth extended beam-to-girder shear tab connections occurs due to the interaction of axial and shear forces at the critical section of the stiffened portion of the shear tab.
- The magnitude of forces, developed at the critical section of the shear plate, depends greatly on the flexibility of the girder web as well the relative distance between the girder bottom flange and the bottom edge of the extended part of the shear plate.
- Implementation of a double-sided configuration of the extended shear tab increases the out-of-plane stiffness of the girder web and decreases the axial demands on the critical section of the stiffener, which leads to higher shear capacity of the connection as compared to single-sided shear tabs.
- Use of a slender shear plate can result in instability of the stiffener soon after local yielding at the critical section; as such, the connection reaches its plateau of strength soon after the yielding of its stiffener.
- The proposed new detailing, in which the shear tab is extended to the bottom K-area of the girder web to facilitate the fabrication procedure, can reach the same level of shear force as compared to the shear tab incorporating current detailing if the b/t compactness limit is met.

Acknowledgments

The authors would like to thank the ADF Group Inc. and DPHV Structural Consultants for their generous technical and financial support, as well as the Natural Sciences and Engineering Research Council of Canada. The finite element computations were conducted at the McGill University's supercomputer Guillimin, which is managed by Calcul Québec and Compute Canada. The supercomputer operation is funded by the Canada Foundation for Innovation (CFI),

NanoQuébec, RMGA and the Fonds de recherche du Québec - Nature et technologies (FRQ-NT).

References

- AISC (2011). "Steel Construction Manual, 14th edition". American Institute of steel Construction, Chicago, IL.
- Cheng, J.-J., Yura, J., Johnson C. (1984). "Design and behavior of coped beams", University of Texas at Austin, Austin, TX.
- CISC (2016). "Handbook of Steel Construction". 11th Edition. Canadian Institute of Steel Construction, Markham, ON.
- CSA-S16 (2014). "Design of Steel Structures". Canadian Standards Association, Mississauga, ON.
- Goldstein Apt, N. (2015). "Testing of extended shear tab and coped beam-to-girder connections subject to shear loading". Master's Thesis, McGill University, Montreal, QC.
- Goodrich, W. (2005). "Behavior of extended shear tabs in stiffened beam-to-column web connections". M.Sc. Thesis, Vanderbilt University, Nashville, TN.
- Hertz, J. (2014). "Testing of extended shear tab connections subjected to shear". Master's Thesis, McGill University, Montreal, QC.
- Hertz, J., Lignos, D.G., Rogers, C.A. (2015). "Full scale testing of extended beam-to-column and beam to-girder shear tab connections subjected to shear", *8th International Conference on Behavior of Steel Structures in Seismic Areas*, Shanghai, China. Paper No. 118.
- Motallebi, M., Lignos, D.G., Rogers, C.A. (2016). "Finite element simulation of buckling of extended beam-to-girder shear tab connections under gravity induced shear force". *Annual Stability Conference of Structural Stability Research Council*, Orlando, FL. Paper No. 14.
- Sherman, D. R., Ghorbanpoor, A. (2002). "Design of extended shear tabs", University of Wisconsin-Milwaukee, Milwaukee, WI.